ELSEVIER

Computational Materials Science 16 (1999) 176–185

COMPUTATIONAL MATERIALS SCIENCE

Simulation of strain localization with gradient enhanced damage models

Ellen Kuhl *, Ekkehard Ramm

Institute of Structural Mechanics, University of Stuttgart, Pfaffenwaldring 7, 70550 Stuttgart, Germany

Abstract

The incorporation of higher order strain gradients into the constitutive equations of continuum damage mechanics is presented. Thereby, not only scalar-valued isotropic damage models but also anisotropic damage models allowing for directional dependent stiffness degradation are elaborated. An elegant possibility of describing anisotropic material behavior based on the microplane theory is demonstrated. Its conceptual simplicity originates from the idea of modeling the material behavior through uniaxial stress–strain laws on several individual material planes. For each plane individual damage loading functions are introduced allowing for different failure modes. In order to account for long ranging microstructural mechanisms, second-order gradients of the strains are incorporated in each of these damage loading functions. The overall response can be determined by an integration of the resulting microplane laws over the solid angle. The features of gradient enhanced continuum damage are demonstrated by means of several selected examples.

Keywords: Continuum damage mechanics; Localization; Gradient continuum; Failure induced anisotropy; Microplane theory; Finite element method

1. Introduction

Many engineering materials consist of various components with different properties. Concrete, for example, is composed of stiff aggregate grains embedded in a relatively weak matrix of mortar. When such heterogeneous materials are subjected to loading, microcracking generally starts at the interface between the different constituents. Upon further loading, the growth and coalescence of these microscopic cracks result in macroscopic crack patterns leading to an overall stiffness degradation. Consequently, the failure mechanism of multiphase materials is of highly anisotropic nature.

The microplane theory derived in [5,8,9,12] represents a powerful approach to describe the above failure phenomena in a natural fashion. Directional dependent stiffness degradation is modeled through uniaxial damage laws on individual potential failure planes leading to a macroscopically anisotropic damage formulation. Different damage laws for tension, compression and shear take into account the different behavior of concrete in mode I, mode II and mixed mode failure.

Due to the heterogeneity of the microstructure, long ranging mechanisms such as microcrack interaction and aggregate interlock severely influ-

* Corresponding author. Tel.:+49-0711-685-6576.
E-mail addresses: khul@statik.uni-stuttgart.de (E. Kuhl), eramm@statik.uni-stuttgart.de (E. Ramm).

0927-0256/99/$ - see front matter
PII: S0927-0256(99)00060-9

ence the stress state at a material point, see [2,16]. Consequently, classical continuum models based on the assumption, that the stress state only depends on the state of the material point itself are no longer sufficient to cover this characteristic behavior. To account for long ranging microstructural effects, the introduction of nonlocal quantities in the constitutive formulation has been proposed, compare [10,11] for example. From the early 1970s on, these nonlocal terms were introduced through an integral equation, see [4,19]. Since the additional integral equation leads to numerically inefficient solution techniques, it has been replaced by a partial differential equation as proposed in [1,6,7]. In the context of continuum damage mechanics, this additional equation defines nonlocal strains which are incorporated in the constitutive relation exclusively through the loading function, see [17]. As a consequence of this enhancement, the resulting equations remain well-posed even in the post-critical regime and the local loss of ellipticity, which is an essential drawback of classical continuum models, is avoided.

After briefly summarizing the constitutive equations of continuum damage mechanics, the derivation of an isotropic gradient enhanced damage model as proposed in [18] will be presented. The regularizing influence of additional gradient terms will be demonstrated by means of the model example of a tension bar. Furthermore, the application of the gradient enhancement in combination with an anisotropic damage model as shown in [13] will be elaborated and illustrated with the help of several selected examples.

2. Classical isotropic damage models and strain localization

The simplest form of continuum damage mechanics is realized through isotropic damage models as described in detail in [14]. Damage is represented by a scalar-valued damage variable d characterizing the reduction of the net stress carrying cross section area fraction. In the following, we will briefly summarize the constitutive equations of isotropic damage restricting ourselves to the small strain case. Consequently, the strain $\boldsymbol{\epsilon}$ is given as the symmetric part of the displacement gradient $\nabla \boldsymbol{u}$

$$\boldsymbol{\epsilon} = \nabla^{\mathrm{sym}} \boldsymbol{u}. \tag{1}$$

Moreover, the free Helmholtz energy Ψ is specified as follows,

$$\begin{aligned} \Psi &= \hat{\Psi}(\boldsymbol{\epsilon}, d, \kappa) \\ &= [1-d]\ 1/2\ \boldsymbol{\epsilon} : \boldsymbol{C}^{\mathrm{el}} : \boldsymbol{\epsilon} + \int_0^{\kappa} \phi(\kappa)\, \mathrm{d}\hat{\kappa}, \end{aligned} \tag{2}$$

whereby $\boldsymbol{C}^{\mathrm{el}} = 2\mu \mathscr{I} + \lambda \mathbf{1} \otimes \mathbf{1}$ denotes the fourth-order elasticity tensor which can be expressed in terms of the Lamé constants μ and λ and the second- and fourth-order unit tensors $\mathbf{1}$ and $\mathscr{I}$. The second term, $\int_0^{\kappa} \phi(\kappa)\, \mathrm{d}\hat{\kappa}$, accounts for the hardening behavior in terms of an additional internal variable κ. The evaluation of the Clausius–Duhem inequality yields the definition of the stress tensor $\boldsymbol{\sigma}$ as thermodynamically conjugate variable to the strain tensor $\boldsymbol{\epsilon}$

$$\boldsymbol{\sigma} = \partial_{\boldsymbol{\epsilon}} \Psi = [1-d] \boldsymbol{C}^{\mathrm{el}} : \boldsymbol{\epsilon} \tag{3}$$

and the energy release rate Y as conjugate variable to the damage variable d.

$$Y = -\partial_d \Psi = 1/2\ \boldsymbol{\epsilon} : \boldsymbol{C}^{\mathrm{el}} : \boldsymbol{\epsilon}. \tag{4}$$

Furthermore, a damage loading function Φ is introduced in the following fashion.

$$\Phi(Y, \phi(\kappa)) = \varphi(Y) - \phi(\kappa) \leqslant 0. \tag{5}$$

It yields the evolution equations of damage and the internal variable in terms of the plastic multiplier $\dot{\gamma}$

$$\dot{d} = \dot{\gamma} \partial_Y \varphi, \quad \dot{\kappa} = \dot{\gamma} \tag{6}$$

and the Kuhn–Tucker conditions which govern the loading/unloading process.

$$\Phi \leqslant 0, \quad \dot{\gamma} \geqslant 0, \quad \Phi \dot{\gamma} = 0. \tag{7}$$

The consistency condition

$$\dot{\Phi} \dot{\gamma} = 0 \tag{8}$$

is evaluated according to [20] with the additional assumption that $\varphi(\cdot) \equiv \phi(\cdot)$. Consequently, the damage variable can be expressed explicitly in terms of a threshold value κ^0 and the maximum

value of the energy release rate that has been obtained so far during the loading history.

$$d = \phi(\kappa)$$
$$\text{with } \kappa = \max_{-\infty<t<\tau} \left(\left[1/2\ \epsilon(t) : \boldsymbol{C}^{\text{el}} : \epsilon(t) \right], \kappa^0 \right). \tag{9}$$

For the example below, we will apply the following specific choice of the equivalent strain φ

$$\varphi(Y) = \sqrt{1/E\,Y} = \sqrt{1/2E\,\epsilon : \boldsymbol{C}^{\text{el}} : \epsilon} \tag{10}$$

and an exponentially softening damage law as proposed in [18].

$$d = \phi(\kappa)$$
$$= 1 - \frac{\kappa^0}{\kappa}[1 - \alpha + \alpha \exp[-\eta[\kappa - \kappa_0]]]. \tag{11}$$

Example 1. To motivate the additional incorporation of nonlocal terms in the constitutive equations, we will demonstrate the incapability of classical continuum models to reproduce correctly the phenomenon of strain localization. Therefore, a bar of $l = 10$ cm length and $h = 1$ cm height is analyzed under tensile loading. The Lamé constants are chosen to be $\mu = 8333.33$ N/mm^2 and $\lambda = 5555.55$ N/mm^2, respectively. The additional material parameters associated with the damage evolution law are chosen in accordance with [18] such that $\alpha = 0.96$ and $\eta = 350$.

Furthermore, the damage threshold value κ_0 is assumed to be $\kappa_0 = 0.0001$ throughout the bar except for a 1 cm wide zone in the middle of the bar, where κ_0 has been reduced by 10% in order to trigger localization. The related load displacement curves for a discretization with 10, 20 and 40 elements are depicted in Fig. 1. Obviously, the brittleness of the specimen increases with increased mesh refinement. This observation, which is of course physically incorrect, is in accordance with the strain distribution depicted in Fig. 2. The strains tend to localize in a narrow zone which is governed by the choice of discretization. Mathematically, this well-known phenomenon of the mesh-dependency of the simulation corresponds to the loss of well-posedness of the governing equations.

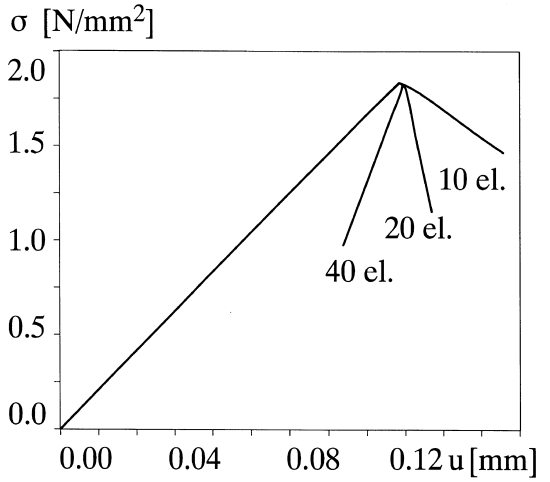

Fig. 1. Isotropic damage – load displacement curves.

3. Isotropic gradient damage

The loss of uniqueness in the post-critical regime which was demonstrated in the previous

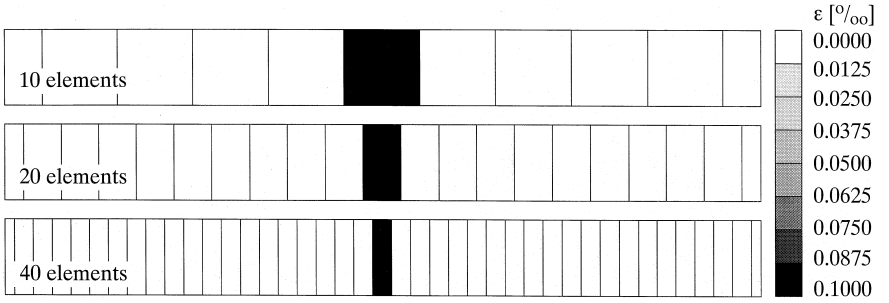

Fig. 2. Isotropic damage – strain distributions.

section can be avoided by introducing a localization limiter in the constitutive equations. Physically, this enhancement is motivated by the heterogeneity of the microstructure leading to long ranging mechanisms on the microstructural scale. An efficient way of realizing this nonlocal enrichment is the introduction of higher order gradients in the damage loading function as proposed by [7,18,17] such that Eq. (5) is replaced by the following damage loading function:

$$\Phi = \varphi(\bar{\epsilon}) - \phi(\kappa) \leqslant 0 \quad \text{with } \varphi(\bar{\epsilon}) = \sqrt{1/2E\ \bar{\epsilon} : \boldsymbol{C}^{\text{el}} : \bar{\epsilon}}. \tag{12}$$

Note, that the equivalent strain φ is no longer a function of the local energy release rate Y. Instead, it has become a function of the nonlocal strain $\bar{\epsilon}$ yielding a nonassociated damage formulation. Consequently, the damage variable defined in Eq. (9) becomes a function of the nonlocal strains as well.

$$d = \phi(\kappa) \quad \text{with } \kappa = \max_{-\infty<t<\tau} \Big(\Big[1/2\ \bar{\epsilon}(t) : \boldsymbol{C}^{\text{el}} : \bar{\epsilon}(t) \Big], \kappa^0 \Big). \tag{13}$$

In order to determine this nonlocal strain field, in addition to the classical *equilibrium problem*

$$\nabla \cdot \boldsymbol{\sigma} = -\rho\ \boldsymbol{b} \quad \text{in } \Omega \tag{14}$$

the following *nonlocal strain problem* is introduced:

$$\nabla \cdot \boldsymbol{\alpha} - \bar{\epsilon} = -\epsilon \quad \text{in } \Omega. \tag{15}$$

For its derivation, which was motivated by the nonlocal integral continuum model, the reader is referred to [18]. For both equations, boundary conditions have to be introduced. For the equilibrium problem, the boundary Γ is divided into disjoint parts $\Gamma_u \cup \Gamma_t = \Gamma$ and $\Gamma_u \cap \Gamma_t = \emptyset$ with the boundary conditions of Dirichlet and Neumann type given as follows,

$$\boldsymbol{u} = \boldsymbol{u}^p \quad \text{on } \Gamma_u, \qquad \boldsymbol{\sigma} \cdot \boldsymbol{n} = \boldsymbol{t}^p \quad \text{on } \Gamma_t. \tag{16}$$

Furthermore, the boundary conditions of the nonlocal strain problem on the boundary Γ with $\Gamma_{\bar{\epsilon}} \cup \Gamma_g = \Gamma$ and $\Gamma_{\bar{\epsilon}} \cap \Gamma_g = \emptyset$ are given by

$$\bar{\epsilon} = \bar{\epsilon}^p \quad \text{on } \Gamma_{\bar{\epsilon}}, \qquad \boldsymbol{\alpha} \cdot \boldsymbol{n} = \boldsymbol{g}^p \quad \text{on } \Gamma_g, \tag{17}$$

whereby in the following, we will only apply the natural boundary condition (17.2). The constitutive equations of the equilibrium problem derived in the previous chapter are summarized in Table 1. Note, that a coupling between the equilibrium problem and the nonlocal strain problem is introduced exclusively in terms of the equivalent strain φ. For the nonlocal strain problem, an additional set of 'constitutive equations' has to be introduced. These equations given in Table 2 relate the nonlocal strain gradient $\boldsymbol{\omega}$ to its conjugate variable $\boldsymbol{\alpha}$ through the definition of an additional potential Ψ^{Ω}. It can be expressed in terms of the tensor $\boldsymbol{P}$ quantifying the influence of the gradient term. In its easiest form, $\boldsymbol{P}$ can be introduced as $\boldsymbol{P} = \text{diag}[c]$ with the gradient parameter c which has the dimension of a length squared. For the parameter identification of the gradient parameter the reader is referred to [15].

The governing equations (14) and (15) are solved numerically with the finite element method. After the application of the partial integration, the divergence theorem and the introduction of the boundary conditions, the weak form of the equilibrium problem reads

$$\int_{\Omega} \nabla \boldsymbol{w}_u^{\text{T}} \boldsymbol{\sigma}\, \text{d}\Omega = \int_{\Omega} \boldsymbol{w}_u^{\text{T}} \rho \boldsymbol{b}\, \text{d}\Omega + \int_{\Gamma} \boldsymbol{w}_u^{\text{T}} \boldsymbol{t}\, \text{d}\Gamma \quad \forall \boldsymbol{w}_u \in \boldsymbol{W}_u, \tag{18}$$

Table 1
Constitutive equations for equilibrium problem – isotropic gradient damage

Kinematics	$\epsilon = \nabla^{\text{sym}} \boldsymbol{u}$
Potential	$\Psi^{\epsilon} = [1-d]\ 1/2\epsilon : \boldsymbol{C}^{\text{el}} : \epsilon + \int_0^{\kappa} \phi(\kappa)\, \text{d}\hat{\kappa}$
Stresses	$\boldsymbol{\sigma} = \partial_{\epsilon} \Psi^{\epsilon} = [1-d] \boldsymbol{C}^{\text{el}} : \epsilon$
Damage loading function	$\Phi = \varphi(\bar{\epsilon}) - \phi(\kappa) \quad \text{with } \varphi = \sqrt{1/2E\bar{\epsilon} : \boldsymbol{C}^{\text{el}} : \bar{\epsilon}}$
Loading/unloading conditions	$\Phi \leqslant 0 \quad \dot{\gamma} \geqslant 0 \quad \Phi\dot{\gamma} = 0$
Damage evolution	$d = \phi(\kappa) \quad \text{with } \kappa = \max_{-\infty<t<\tau} \big(\big[1/2\bar{\epsilon} : \boldsymbol{C}^{\text{el}} : \bar{\epsilon} \big], \kappa^0 \big)$

Table 2
Constitutive equations for nonlocal strain problem

Kinematics	$\boldsymbol{\omega} = \nabla\bar{\epsilon}$
Potential	$\Psi^{\Omega} = 1/2\ \boldsymbol{\omega}\cdot\boldsymbol{P}\cdot\boldsymbol{\omega}$
Conjugate variable	$\boldsymbol{\alpha} = \partial_{\omega}\Psi^{\Omega} = \boldsymbol{P}\cdot\boldsymbol{\omega}$

whereas the weak form of the nonlocal strain problem is given as follows,

$$\int_{\Omega} \nabla \boldsymbol{w}_{\bar{\epsilon}}^{\mathrm{T}}\boldsymbol{\alpha}\,\mathrm{d}\Omega + \int_{\Omega} \boldsymbol{w}_{\bar{\epsilon}}^{\mathrm{T}}\bar{\boldsymbol{\epsilon}}\,\mathrm{d}\Omega = \int_{\Omega} \boldsymbol{w}_{\bar{\epsilon}}^{\mathrm{T}}\boldsymbol{\epsilon}\,\mathrm{d}\Omega + \int_{\Gamma} \mathbf{w}_{\bar{\epsilon}}^{\mathrm{T}}\boldsymbol{g}\,\mathrm{d}\Gamma \quad \forall \boldsymbol{w}_{\bar{\epsilon}} \in \boldsymbol{W}_{\bar{\epsilon}}. \tag{19}$$

Herein, $\boldsymbol{w}_u$ and $\boldsymbol{w}_{\bar{\epsilon}}$ denote the weightening functions and $\rho\boldsymbol{b}$ represents the applied volume forces. The discretization is performed by applying independent discretizations of the displacement field $\boldsymbol{u}$ and the nonlocal strain field $\bar{\boldsymbol{\epsilon}}$,

$$\boldsymbol{u} = \boldsymbol{N}_u\boldsymbol{d}_u, \quad \boldsymbol{\epsilon} = \boldsymbol{B}_u\boldsymbol{d}_u, \quad \bar{\boldsymbol{\epsilon}} = \boldsymbol{N}_{\bar{\epsilon}}\boldsymbol{d}_{\bar{\epsilon}}, \quad \nabla\bar{\boldsymbol{\epsilon}} = \boldsymbol{B}_{\bar{\epsilon}}\boldsymbol{d}_{\bar{\epsilon}} \tag{20}$$

with $\boldsymbol{N}$ and $\boldsymbol{B}$ representing the individual shape functions and their spatial derivatives whereas $\boldsymbol{d}_u$ and $\boldsymbol{d}_{\bar{\epsilon}}$ are the nodal degrees of freedom. A linearization yields the following set of equations

$$\int_{\Omega} \boldsymbol{B}_u^{\mathrm{T}}\tilde{\boldsymbol{C}}_{i-1}\boldsymbol{B}_u\Delta\boldsymbol{d}_u\,\mathrm{d}\Omega + \int_{\Omega} \boldsymbol{B}_u^{\mathrm{T}}\Delta\tilde{\boldsymbol{C}}\boldsymbol{N}_{\bar{\epsilon}}\Delta\mathbf{d}_{\bar{\epsilon}}\,\mathrm{d}\Omega = \int_{\Omega} \boldsymbol{N}_u^{\mathrm{T}}\rho\boldsymbol{b}\,\mathrm{d}\Omega + \int_{\Gamma} \boldsymbol{N}_u^{\mathrm{T}}\boldsymbol{t}\,\mathrm{d}\Gamma - \int_{\Omega} \boldsymbol{B}_u^{\mathrm{T}}\boldsymbol{\sigma}_{i-1}\,\mathrm{d}\Omega,$$

$$\int_{\Omega} \boldsymbol{N}_{\bar{\epsilon}}^{\mathrm{T}}\boldsymbol{B}_u\Delta\boldsymbol{d}_u\,\mathrm{d}\Omega + \int_{\Omega} \left[\boldsymbol{N}_{\bar{\epsilon}}^{\mathrm{T}}\boldsymbol{N}_{\bar{\epsilon}} + \boldsymbol{B}_{\bar{\epsilon}}^{\mathrm{T}}\boldsymbol{P}_{i-1}\boldsymbol{B}_{\bar{\epsilon}}\right]\Delta\mathbf{d}_{\bar{\epsilon}}\,\mathrm{d}\Omega = \int_{\Omega} \left[\left[\boldsymbol{N}_{\bar{\epsilon}}^{\mathrm{T}}\boldsymbol{N}_{\bar{\epsilon}} + \boldsymbol{B}_{\bar{\epsilon}}^{\mathrm{T}}\boldsymbol{P}_{i-1}\boldsymbol{B}_{\bar{\epsilon}}\right]\boldsymbol{d}_{\bar{\epsilon},i-1} - \boldsymbol{N}_{\bar{\epsilon}}^{\mathrm{T}}\boldsymbol{\epsilon}_{i-1}\right]\mathrm{d}\Omega,$$

which can be solved for the incremental update of the nodal degrees of freedom $\Delta\boldsymbol{d}_u$ and $\Delta\boldsymbol{d}_{\bar{\epsilon}}$ by an incremental iterative Newton–Raphson solution procedure after assembling the global system of equations.

Example 2. The regularizing influence of the additional gradient term will be demonstrated by analyzing Example 1 with a gradient enhanced continuum damage model. The geometry and the material parameters are identical to the ones given in Example 1. In addition, the gradient parameter

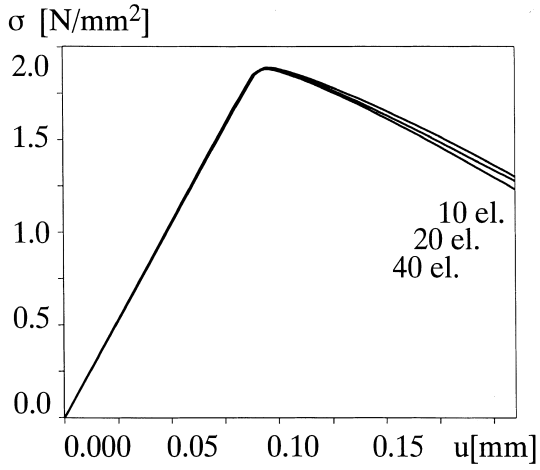

Fig. 3. Isotropic gradient damage – load displacement curves.

c is chosen to $c = 2$ cm^2. The load displacement curves depicted in Fig. 3 show an almost identical response for the three different discretizations. Due to the inclusion of higher order gradients in the damage loading function, the results seem to be independent of the underlying discretization. The distribution of the nonlocal strains given in Fig. 4 confirms this observation. The width of the affected zone is governed by the choice of the gradient parameter c. Remarkably, the width of the affected zone remains constant upon mesh refinement.

4. Anisotropic gradient damage

In the following, an anisotropic damage model motivated by the microplane concept will be introduced. The basic ideas of the microplane model are adopted from the well-known theory of crystal plasticity, for which the overall anisotropic response can be derived by evaluating uniaxial plastic laws on selected material planes. These planes, the so-called slip planes, are predefined by the geometry of the crystallographic lattice as depicted in Fig. 5. In the microplane theory, the plastic laws are replaced by uniaxial damage laws. Moreover,the definition of the potential failure planes is not known in advance. Therefore, as many planes as possible have to be taken into

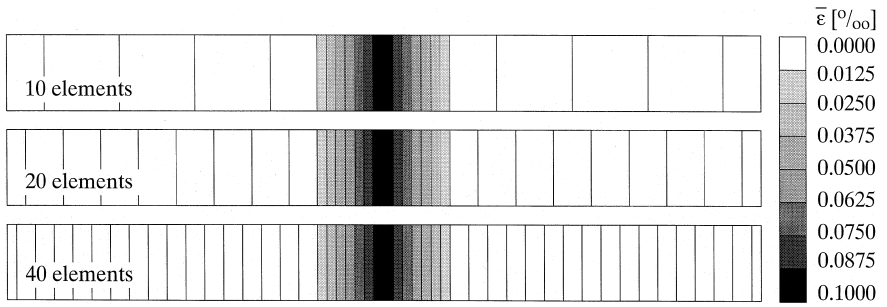

Fig. 4. Isotropic gradient damage – nonlocal strain distributions.

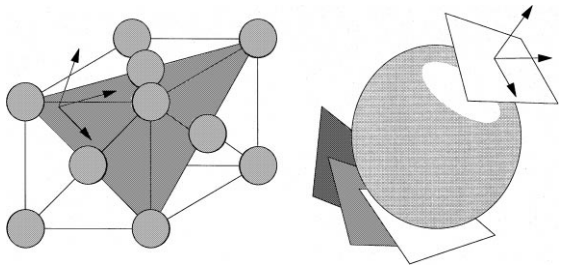

Fig. 5. Analogy between crystal plasticity and microplane model.

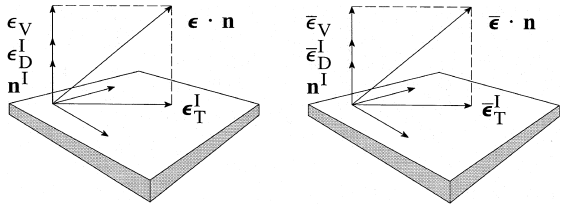

Fig. 6. Strain components on one microplane.

account in order to reproduce correctly the actual stress state. The microplane model derived in the following is based on a so-called 'kinematic constraint'. The local and nonlocal strain components of a microplane are determined by projecting the local and the nonlocal macroscopic strain tensor onto the material plane as sketched in Fig. 6. Consequently, the individual volumetric, deviatoric and tangential strain components of one individual plane can be expressed as follows:

$$\begin{aligned}
&\epsilon_V = \boldsymbol{\epsilon} : \boldsymbol{V}, \quad \bar{\epsilon} = \bar{\boldsymbol{\epsilon}} : \boldsymbol{V}, \quad \boldsymbol{V} = \tfrac{1}{3}\mathbf{1}, \\
&\epsilon_D = \boldsymbol{\epsilon} : \boldsymbol{D}, \quad \bar{\epsilon}_D = \bar{\boldsymbol{\epsilon}} : \boldsymbol{D}, \quad \boldsymbol{D} = \boldsymbol{n} \otimes \boldsymbol{n} - \boldsymbol{V}, \\
&\epsilon_T = \boldsymbol{\epsilon} : \boldsymbol{T}, \quad \bar{\epsilon}_T = \bar{\boldsymbol{\epsilon}} : \boldsymbol{T}, \quad \boldsymbol{T} = \mathscr{I} \cdot \boldsymbol{n} - \boldsymbol{n} \otimes \boldsymbol{n} \otimes n.
\end{aligned} \tag{21}$$

Herein, $\boldsymbol{V}$, $\boldsymbol{D}$and $\boldsymbol{T}$denote the second- and third-order projection tensors characterized by the plane's normal $\boldsymbol{n}$. As indicated in the previous section, the damage loading functions will be introduced as functions of the nonlocal strains $\bar{\epsilon}_V, \bar{\epsilon}_D$ and $\bar{\epsilon}_T$ and the history parameters κ_V, κ_D and κ_T. Different damage loading functions are formulated for each component in order to account for the different failure modes.

$$\begin{aligned}
&\Phi_V = \varphi(\bar{\epsilon}_V) - \phi(\kappa_V), \qquad \Phi_D = \varphi(\bar{\epsilon}_D) - \phi(\kappa_D), \\
&\Phi_T = \varphi(\bar{\epsilon}_T) - \phi(\kappa_T).
\end{aligned} \tag{22}$$

The evaluation of the loading/unloading conditions and the consistency condition

$$\begin{aligned}
&\Phi_V \leqslant 0, \quad \dot{\gamma}_V \geqslant 0, \quad \Phi_V \dot{\gamma}_V = 0, \quad \dot{\Phi}_V \dot{\gamma}_V = 0, \\
&\Phi_D \leqslant 0, \quad \dot{\gamma}_D \geqslant 0, \quad \Phi_D \dot{\gamma}_D = 0, \quad \dot{\Phi}_D \dot{\gamma}_D = 0, \\
&\Phi_T \leqslant 0, \quad \dot{\gamma}_T \geqslant 0, \quad \Phi_T \dot{\gamma}_T = 0, \quad \dot{\Phi}_T \dot{\gamma}_T = 0,
\end{aligned} \tag{23}$$

yields the values of the individual history parameters κ_V, κ_D and κ_T describing the largest amount of straining, the individual component has experienced so far. The history parameters govern the evolution of the damage variables d_V, d_D and d_T.

$$\begin{aligned}
&d_V = \phi_V(\kappa_V), \quad d_D = \phi_D(\kappa_D), \\
&d_T = \phi_T(\kappa_T).
\end{aligned} \tag{24}$$

The individual microplane stress components are thus given by uniaxial damage laws of the following form.

$$\sigma_V = [1 - d_V]C_V\epsilon_V, \quad \sigma_D = [1 - d_D]C_D\epsilon_D,$$
$$\boldsymbol{\sigma}_T = [1 - d_T]C_T\boldsymbol{\epsilon}_T. \tag{25}$$

An integration of all the stress components of all directions over the solid angle Ω yields the homogenized stress tensor $\boldsymbol{\sigma}$ in terms of the individual microplane stress components σ_V, σ_D and $\boldsymbol{\sigma}_T$.

$$\boldsymbol{\sigma} = \frac{3}{4\pi}\int_\Omega \left[\sigma_V \boldsymbol{V} + \sigma_D \boldsymbol{D} + \boldsymbol{\sigma}_T \cdot \boldsymbol{T}^T\right] d\Omega. \tag{26}$$

The constitutive equations of anisotropic microplane damage are summarized in Table 3. For the initial case of *isotropic elasticity* with $d_V = d_D = d_T \equiv 0$ the combination of Eqs. (25) and (26) yields the definition of the stress tensor of elastic material behavior as a special case of Eq. (26).

$$\boldsymbol{\sigma} = \frac{3}{4\pi}\int_\Omega \left[C_V\epsilon_V \boldsymbol{V} + C_D\epsilon_D \boldsymbol{D} + C_T\boldsymbol{\epsilon}_T \cdot \boldsymbol{T}^T\right] d\Omega. \tag{27}$$

With the help of the kinematic constraint defined in Eq. (21), Eq. (27) can be rewritten as follows.

$$\boldsymbol{\sigma} = \boldsymbol{C} : \boldsymbol{\epsilon},$$
$$C = \frac{3}{4\pi}\int_\Omega \left[C_V \mathbf{V} \otimes \boldsymbol{V} + C_D \boldsymbol{D} \otimes \boldsymbol{D} + C_T \boldsymbol{T} \cdot \boldsymbol{T}^T\right] d\Omega. \tag{28}$$

The products of the projection tensors $\boldsymbol{V}$, $\boldsymbol{D}$ and $\mathbf{T}$ can be integrated analytically over the solid angle Ω by applying the integration formulae summarized in [8].

$$\frac{3}{4\pi}\int_\Omega \boldsymbol{V} \otimes \boldsymbol{V}\, d\Omega = \mathscr{I}^{vol},$$
$$\frac{3}{4\pi}\int_\Omega \boldsymbol{D} \otimes \boldsymbol{D}\, d\Omega = \frac{2}{5}\mathscr{I}^{dev}, \tag{29}$$
$$\frac{3}{4\pi}\int_\Omega \boldsymbol{T} \cdot \boldsymbol{T}\, d\Omega = \frac{3}{5}\mathscr{I}^{dev}.$$

A comparison with Hooke's elasticity tensor $\boldsymbol{C}^{el} = 2\mu\mathscr{I} + \lambda\mathbf{1} \otimes \mathbf{1}$ yields the definition of the microplane elasticity moduli C_V, C_D and C_T in terms of the Lamé constants μ and λ.

$$C_V = 3\lambda + 2\mu = 3\kappa, \quad \tfrac{2}{5}C_D + \tfrac{3}{5}C_T = 2\mu. \tag{30}$$

For the general *anisotropic* case the damage variables are allowed to be larger than zero. Furthermore, they can be different for different directions depending on the plane's normal $\boldsymbol{n}$ such that $d_V(\boldsymbol{n}) \neq 0, d_D(\boldsymbol{n}) \neq 0$ and $d_T(\boldsymbol{n}) \neq 0$. In that case, an analytical evaluation of the macroscopic stress state is nearly impossible. However, a numerical evaluation of Eq. (26) can be performed. The integral expression $(3/4\pi)\int_\Omega f\, d\Omega$ is thus approximated by a weighted sum $\sum_{I=1}^{nmp} f^I w^I$ of the function f evaluated at discrete integration points and weighted by the weightening coefficient w^I. Eq. (26) can thus be approximated by the following relation.

$$\begin{aligned}\boldsymbol{\sigma} = \sum_{I=1}^{nmp} \Big[&\left[1 - d_V^I\right] C_V\, \mathbf{V}^I \otimes \boldsymbol{V}^I \\ &+ \left[1 - d_D^I\right] C_D\, \boldsymbol{D}^I \otimes \boldsymbol{D}^I \\ &+ \left[1 - d_T^I\right] C_T\, \boldsymbol{T}^I \cdot \mathbf{T}^{I\,T}\Big] w^I : \boldsymbol{\epsilon}.\end{aligned} \tag{31}$$

It was shown in [3] that the numerical integration with $nmp = 21$ integration points per hemisphere

Table 3
Constitutive equations for equilibrium problem – anisotropic damage

Macroscopic strains	$\boldsymbol{\epsilon} = \nabla^{sym}\boldsymbol{u}$		
Microplane strains	$\epsilon_V = \boldsymbol{\epsilon} : \boldsymbol{V}$	$\epsilon_D = \boldsymbol{\epsilon} : \boldsymbol{D}$	$\epsilon_T = \boldsymbol{\epsilon} : \boldsymbol{T}$
	$\bar{\epsilon}_V = \bar{\boldsymbol{\epsilon}} : \boldsymbol{V}$	$\bar{\epsilon}_D = \bar{\boldsymbol{\epsilon}} : \boldsymbol{D}$	$\epsilon_T = \bar{\boldsymbol{\epsilon}} : \boldsymbol{T}$
Macroscopic stresses	$\boldsymbol{\sigma} = \int_\Omega [\sigma_V \boldsymbol{V} + \sigma_D \boldsymbol{D} + \boldsymbol{\sigma}_T \cdot \boldsymbol{T}^T]\, d\Omega$		
Microplane stresses	$\sigma_V = [1 - d_V]C_V\epsilon_V$	$\sigma_D = [1 - d_D]C_D\epsilon_D$	$\boldsymbol{\sigma}_T = [1 - d_T]C_T\boldsymbol{\epsilon}_T$
Damage functions	$\Phi_V = \varphi(\bar{\epsilon}_V) - \phi(\kappa_V)$	$\Phi_D = \varphi(\bar{\epsilon}_D) - \phi(\kappa_D)$	$\Phi_T = \varphi(\bar{\epsilon}_T) - \phi(\kappa_T)$
Loading/unloading	$\Phi_V \leqslant 0$	$\Phi_D \leqslant 0$	$\Phi_T \leqslant 0$
	$\dot{\gamma}_V \geqslant 0$	$\dot{\gamma}_D \geqslant 0$	$\dot{\gamma}_T \geqslant 0$
	$\Phi_V\dot{\gamma}_V = 0$	$\Phi_D\dot{\gamma}_D = 0$	$\Phi_T\dot{\gamma}_T = 0$
Damage evolution	$d_V = \phi_V(\kappa_V)$	$d_D = \phi_D(\kappa_D)$	$d_T = \phi_T(\kappa_T)$

yields a sufficiently accurate approximation at an acceptable level of effort. In that case, the microplanes are situated as tangential planes to the vertices and edges of a regular icosahedron as indicated in Fig. 7.

Example 3. The features of the anisotropic gradient model will be demonstrated by the analysis of a compression panel. The specimen of $h = 12$ cm height and a width of $w = 6$ cm will be analyzed under plane strain conditions. The Lamé constants are chosen to be $\mu = 12711.86$ N/mm^2 and $\lambda = 7150.42$ N/mm^2. In order to trigger localization, an imperfection has been introduced by reducing the elastic properties by 10% in a 1 cm $\times$ 1 cm large zone in the upper right corner. Except for the volumetric compression, damage laws of an exponential type

$$d(\kappa) = 1 - \exp[[\kappa/a]^p]$$

are applied, introducing two material parameters a and p for each damage law. The material parameters for each component differentiating between tension and compression are chosen to be $a_{\mathrm{V}}^{+} = a_{\mathrm{D}}^{+} = 0.00006, a_{\mathrm{D}}^{-} = 0.0004,\ a_{\mathrm{T}}^{+} = a_{\mathrm{T}}^{-} = 0.0004,\ p_{\mathrm{V}}^{+} = p_{\mathrm{D}}^{+} = 1.0,\ p_{\mathrm{D}}^{-} = 1.2,\ p_{\mathrm{T}}^{+} = p_{\mathrm{T}}^{-} = 1.1$. The damage law for volumetric compression

$$d_{\mathrm{V}}(\kappa_{\mathrm{V}}) = \left[[1 - \kappa_{\mathrm{V}}/a_{\mathrm{V}}]^{-p_{\mathrm{V}}^{-}} + [-\kappa_{\mathrm{V}}/b_{\mathrm{V}}^{-}]^{q_{\mathrm{V}}^{-}}\right]$$

and the related material parameters are chosen as $a_{\mathrm{V}}^{-} = 0.005,\ b_{\mathrm{V}}^{-} = 0.035,\ p_{\mathrm{V}}^{-} = 1.0,\ q_{\mathrm{V}}^{-} = 1.85$.

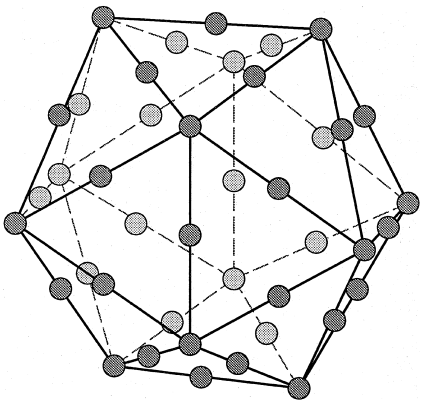

Fig. 7. Numerical integration with $nmp = 21$ integration points per hemisphere.

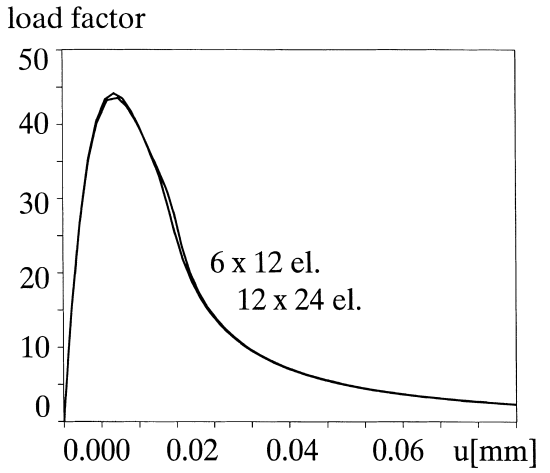

Fig. 8. Load displacement curves of compression panel.

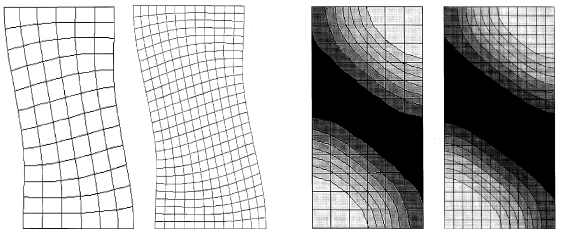

Fig. 9. Deformed configurations and nonlocal strain distribution of compression panel.

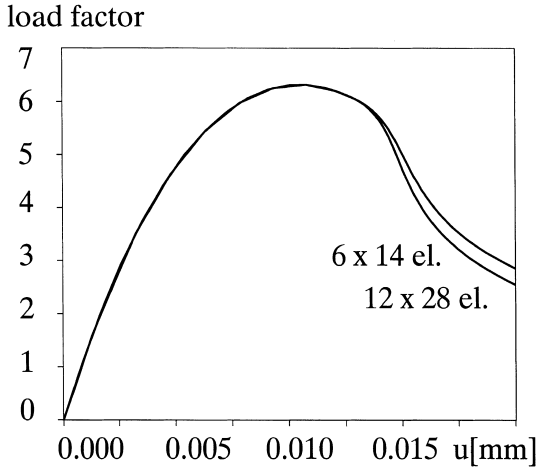

Fig. 10. Load displacement curves of tensile test.

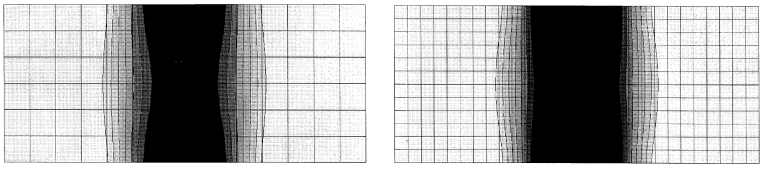

Fig. 11. Distribution of nonlocal strains in tension specimen.

Furthermore, the gradient parameter c is assumed to be $c = 3$ cm^2. Two different discretizations of 72 and 288 elements have been analyzed yielding an almost identical material response as demonstrated by the corresponding load displacement curves of Fig. 8. Fig. 9 shows the deformed configuration and the distribution of the nonlocal strains in loading direction. Obviously, the specimen has failed due to a shear band which has formed under the angle of 45° towards the loading axis. The regularizing influence of the gradient enhancement is once more highlighted by the clear mesh-independency of the results.

Example 4. In the last example, a tensile test of a $l = 14$ cm long and $h = 6$ cm high specimen is simulated. The material parameters are identical to the previous example, except for the gradient parameter which is now chosen as $c = 2.25$ cm^2. An imperfect zone of 1×2 cm^2 has been introduced in the middle of the free edges in order to simulate a double edge notched specimen. Again, two different discretizations with 84 and 336 elements have been studied. The corresponding load displacement curves are depicted in Fig. 10. The solution is found to be independent of the underlying discretization. The distribution of the nonlocal strains in loading direction shown in Fig. 11 confirms this observation. Due to the special choice of damage laws and material parameters, the tension specimen shows a clear mode I failure in contrast to the compression panel of Example 3. The presented examples have not only demonstrated the facility of the gradient enhanced microplane model to reproduce correctly the phenomenon of strain localization, but have also shown its capability of capturing different failure modes through the application of different damage laws for the individual microplane components.

5. Conclusion

Different continuum damage models including a dependence upon the second gradient of the strains have been proposed. Due to the implicit incorporation of an internal length scale, the governing equations remain well-posed even in the post-critical regime. Especially the anisotropic damage model derived in the context of the microplane theory is believed to be very promising for the modeling of different failure modes under various loading scenarios. The related examples have demonstrated the capabilities of the present model to simulate mode I as well as mixed mode failure up to the complete loss of load carrying capacity.

Acknowledgements

The present study is supported by grants of the German National Science Foundation (DFG) within the graduate program 'Modellierung und Diskretisierungsmethoden für Kontinua und Strömungen'. This support is gratefully acknowledged.

References

[1] E. Aifantis, On the role of gradients in the localization of deformation and fracture, Int. J. Eng. Sci. 30 (1992) 1279–1299.
[2] Z. Bažant, Why continuum damage is nonlocal: micromechanics arguments, J. Eng. Mech. 117 (1991) 1070–1087.
[3] Z. Bažant, B. Oh, Microplane model for progressive fracture of concrete and rock, J. Eng. Mech. 111 (1985) 559–582.
[4] Z. Bažant, J. Ožbolt, Nonlocal microplane model for fracture damage and size effect in structures, J. Eng. Mech. 116 (1990) 2485–2505.

[5] Z. Bažant, P. Prat, Microplane model for brittle plastic material: Part I – Theory, Part II – verification, J. Engrg. Mech. 114 (1988) 1672–1702.
[6] R. De Borst, H. Mühlhaus, Gradient-dependent plasticity: formulation and algorithmic aspects, Int. J. Num. Meth. Eng. 35 (1992) 521–539.
[7] R. De Borst, J. Pamin, R. Peerlings, B. Sluys, On gradient-enhanced damage and plasticity models for failure in quasi-brittle and frictional materials, Comput. Mech. 17 (1995) 130–141.
[8] I. Carol, Z. Bažant, Damage and plasticity in microplane theory, Int. J. Solids and Structures 34 (1997) 3807–3835.
[9] I. Carol, P. Prat, Z. Bažant, New explicit microplane model for concrete: Theoretical aspects and numerical implementation, Int. J. Solids and Structures 29 (1992) 1173–1191.
[10] A. Eringen, D. Edelen, On nonlocal elasticity, Int. J. Eng. Science 10 (1972) 233–248.
[11] E. Kröner, Elasticity theory of materials with long range cohesive forces, Int. J. Solids and Structures 3 (1967) 731–742.
[12] E. Kuhl, E. Ramm, On the linearization of the microplane model, Mech. Coh. Frict. Mat, in press.
[13] E. Kuhl, E. Ramm R. DeBorst An anisotropic gradient damage model for quasi-brittle materials, Comp. Meth. Appl. Mech. Eng., accepted.
[14] J. Lenaitre, J. Chaboche, Mechanique des Materiaux Solides, Dunod, Paris, 1988.
[15] R. Mahnken, E. Kuhl, A finite element algorithm for parameter identification of gradient enhanced damage models, Eur. J. Mech. / A: Solids, submitted.
[16] J. Van Mier, Fracture Processes of Concrete, CRC Press, Boca Raton, 1997.
[17] R. Peerlings, R. De Borst, W. Brekelmans, J. Geers, Gradient-enhanced damage modelling of concrete fracture, Mech. Coh. Fric. Mat. 3 (1998) 323–342.
[18] R. Peerlings, R. De Borst, W. Brekelmans, J. Vree, Gradient enhanced damage for quasi-brittle materials, Int. J. Num. Meth. Eng. 39 (1996) 3391–3403.
[19] G. Pijaudier Cabot, Z. Bažant, Nonlocal damage theory, J. Eng. Mech. 113 (1987) 1512–1533.
[20] J. Simo, J. Ju, Strain- and stress based continuum damage models: Part I – Formulation, Part II – Computational aspects, Int. J. Solids and Structures 23 (1987) 821–869.